J Solid State Electrochem (2011) 15:431–445
DOI 10.1007/s10008-010-1117-6

REVIEW

Electrode materials for aqueous rechargeable lithium batteries

H. Manjunatha · G. S. Suresh · T. V. Venkatesha

Received: 5 April 2010 / Revised: 16 May 2010 / Accepted: 24 May 2010 / Published online: 12 June 2010

Abstract In this review, we describe briefly the historical development of aqueous rechargeable lithium batteries, the advantages and challenges associated with the use of aqueous electrolytes in lithium rechargeable battery with an emphasis on the electrochemical performance of various electrode materials. The following materials have been studied as cathode materials: $LiMn_2O_4$, MnO_2, $LiNiO_2$, $LiCoO_2$, $LiMnPO_4$, $LiFePO_4$, and anatase TiO_2. Addition of certain additives like TiS_2, TiB_2, CeO_2, etc. is found to increase the performance of MnO_2 cathode. The following materials have been studied as anode materials: VO_2 (B), LiV_3O_8, LiV_2O_5, $LiTi_2(PO4)_3$, TiP_2O_3, and very recently conducting polymer, polypyrrole (PPy). The cell PPy/$LiCoO_2$, constructed using polypyrrole as anode delivers an average voltage of 0.86 V with a discharge capacity of 47.7 mA hg^{-1}. It retains the capacity for first 120 cycles. The cell, $LiTi_2(PO_4)_3$/1 M Li_2SO_4/$LiMn_2O_4$, delivers a capacity of 40 mA hg^{-1} and specific energy of 60 mW hg^{-1} with an output voltage of 1.5 V over 200 charge–discharge cycles. An aqueous lithium cell constructed using MWCNTs/$LiMn_2O_4$ as cathode material is found to exhibit more than 1,000 cycles with good rate capability.

H. Manjunatha · G. S. Suresh (✉)
Chemistry Research Centre, SSMRV Degree College,
Jayanagar,
Bangalore 560041, India
e-mail: sureshssmrv@yahoo.co.in

T. V. Venkatesha
Department of Chemistry, Kuvempu University,
Jnana Sahyadri,
Shankaraghatta 577451 Shimoga, India

Keywords Aqueous rechargeable lithium battery · Charge transfer reactions · Aqueous electrolytes · Anode materials · Cathode materials · Intercalation/deintercalation processes

Introduction

Development of world's economy and increase in population has resulted in increase in the number of vehicles on the road. Most of these vehicles use fossil fuels that emit green house gases such as CO_2 results in serious pollution of air and environment. One of the possible alternatives to save the environment is to look towards electric vehicles (EVs) that could reduce emission of CO_2. It is well understood that a rechargeable battery with high efficiency (high specific energy, high voltage, and long shelf life), low cost, and good safety is the key factor in the development of practical electric vehicles. The present rechargeable battery technologies use expensive components or assembly technology which is the main drawback for the commercialization and popularization of EVs. Only few battery systems meet the required characteristics. Each battery technology has its own advantages and disadvantages [1–4]. The first detailed account on "rechargeable batteries" was given by Wade [5] in 1902, which deals almost with Pb-PbO_2 system. It was stated by Barak [6] that the lead/acid battery remains to be the "work house" among rechargeable electrochemical power sources. Later Ni-H and Ni-MH batteries with aqueous electrolytes were developed and commercialized. All these battery systems are found to be having low energy density, poor cyclability, and less shelf life. Rechargeable lithium batteries have been attracting the interest of many researchers as possible long-term solution to the electric vehicle's battery problem. This is due to their high energy density, high working potential, and long life [7].

In the mid-1990s, Dahn and his colleagues [8] proposed a new type of rechargeable Li-ion battery using an aqueous electrolyte. Researchers thought this development a breakthrough or big plus because safety goes away as described by Glanze [9] and a possible way for the development of a battery system for electric vehicles. This cell uses $LiMn_2O_4$ as cathode, VO_2 (B) as anode and 5 M $LiNO_3$ in water as electrolyte. Although energy density (cell potential 1.5 V) of this cell is lower than that of non-aqueous systems, it can be compared to that of Pb-acid and Ni-Cd batteries. Dahn and coworkers strategy in using aqueous electrolytes is chemically taming or restraining lithium so that it cannot react with water. This is achieved by using suitable intercalation host in which Li can bind sufficiently tightly (at about 3.2±0.2 eV) so that it will not react with water and then use a simple aqueous electrolyte containing Li salts. Since LiOH is exactly what results when Li reacts with water, loading the electrolyte with the compound saturates the system ruling out further reactions. However in aqueous rechargeable lithium battery systems, one cannot ignore the possibility of proton intercalation instead of Li^+ and there is a need to identify the cation which is intercalated/deintercalated to $LiMn_2O_4$. Later in 1995, Li and Dahn [10] confirmed the insertion of Li^+ into manganese dioxide and rejected any possibility of proton intercalation. If Li^+ deintercalation from $LiMn_2O_4$ and H^+ intercalation into VO_2 (B) is assumed during the charging of $LiMn_2O_4/VO_2$ (B) cell in aqueous solution, then the concentration of H^+ ions in the electrolyte decreases and that of Li^+ ions increases. As a result following reaction takes place preventing Li deintercalation from $LiMn_2O_4$.

$$Li_{1-x}Mn_2O_4 + xLi^+ + xOH^- \rightarrow LiMn_2O_4 + (x/2)H_2O + (x/4)O_2 \quad (1)$$

Oxygen evolution occurs at about 3.5 V vs Li (see Fig. 2), which further prevents Li deintercalation. Despite several advantages with aqueous electrolytes, early lithium-ion cells showed rapid capacity loss with continuous cycling (25 cycles). Zhang and Dahn [11] studied cyclic voltammetry of VO_2 (B) electrode in aqueous solutions of different pH value and revealed that the capacity loss of the cell with cycling is due to the dissolution of anode material in the electrolyte solution. The amount of anode material dissolved was found to depend on the solution pH. As the pH decreased, the hydrogen evolution process is enhanced and this will influence the kinetics of lithium intercalation reaction. Figure 1 shows the specific capacity of VO_2 (B) electrode measured as a function of pH. The capacity loss is much reduced when the pH of the electrolyte is less than 10. This shows that there is a slight increase in the dissolution of VO_2 (B) into electrolytes with increasing pH up to about 10 then it is increased significantly above pH10. Thus VO_2 (B) was found to be stable electrode in the pH range 8–10.

Theory

Dahn and his group [12] studied the thermodynamic stability of lithium intercalation compounds in water/aqueous solutions. A brief summary of their work is presented here. Binding energy of Li in Li (Host) materials is a good measure of their stability. This binding energy is

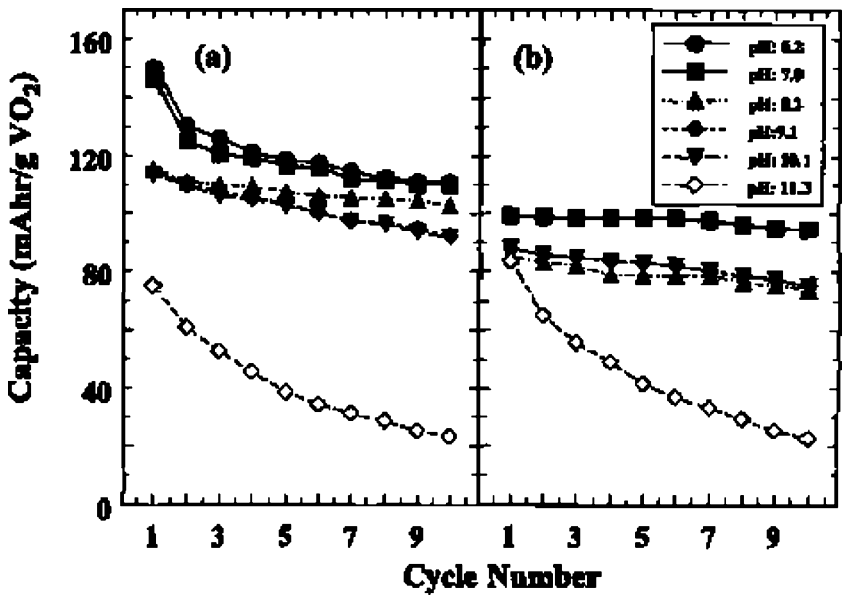

Fig. 1 Variations of the capacities of VO_2 (B) electrode with electrolyte pH [11]. **a** capacity during discharge **b** capacity during charge

equal to the voltage of Li/Li (int) cell. Higher cell voltage corresponds to more tightly bound Li. When Li (int) reacts with H_2O, O_2, and CO_2 the products formed are LiOH, solid Li_2O and solid Li_2CO_3. The free energies of formation of these products are −51, −134 and −176 kcal mol^{-1} respectively. Converting these free energies of formation into binding energies (eV), the values obtained are −2.22, −2.91 and −3.82 eV (with respect to lithium atom). Lithium intercalation compounds with voltages greater than 3.9 V vs Li should be thermodynamically stable with respect to the formation of any of these products. However, this is not so because the materials with somewhat less voltages than 3.9 V are also found to be air stable. From Makinnon and Hearing [13], the chemical potential μ_{Li}^{int} of intercalated Li in Li_x(Host) is given by

$$\mu_{Li}^{int(x)} = \frac{1}{N_A}\frac{(\delta G^{\circ} Li_x(\text{Host}))}{\delta x} \tag{2}$$

Where G^0_{Lix}(Host) is the Gibb's free energy of 1 mole of Li_x(Host) in its standard (solid) state and N_A is the Avogadro's number. Integrating, we have

$$G^{\circ} Li_x(\text{Host}) = G^{\circ}(\text{Host}) + \int_0^x N_A \mu_{Li}^{int}(x)dx \tag{3}$$

Mackinnon and Hearing showed that the voltage $V(x)$ of $Li/Li_{(x)}$(Host) cell is given by

$$V(x) = -1/e\left(\mu_{Li}^{int}{}_{(x)} - \mu^0{}_{Li}\right) \tag{4}$$

Where $\mu_{Li}{}^0$ is the chemical potential of Li metal given by the equation, $\mu^0_{Li} = \left(\delta G^0_{Li}/\delta N\right)$ and e is the magnitude of the electron charge. Applying the above equation for the reaction, $Li(int)+H_2O \leftrightarrow Li^+ + OH^- + (1/2)\ H_2$, they derived the following expression for the voltage vs Li of the Li(int) in contact with water.

$$V(x) = 3.885 - 0.118\text{pH}(V) \tag{5}$$

According to the above expression, Li(int) with voltages $V(x)$ vs Li placed in water will react and the resulting pH will be given by solving the above equation. The same expression can be rewritten for Li(int) with voltage $V(x)$ in equilibrium with LiOH solution as follows

$$V(x) = 2.23 - 2kT\ln[Li^+](V) \tag{6}$$

The meaning of the above expression is very significant in selecting the electrode materials for aqueous rechargeable lithium batteries. If $V(x) > 2.23 - 2kT\ln[Li^+]$, no Li will deintercalate from Li_x(Host) and it will be stable in alkaline solutions. The potential of the Li electrode drops with respect to SHE as the pH decreases. Figure 2 shows a general potential—pH diagram or Pourbaix diagram of variety of Li intercalation compounds in aqueous solutions. In conclusion, the electrochemical intercalation of lithium can occur from aqueous solutions provided that the host materials, Li-ion concentration and pH are carefully selected using the Pourbaix diagram and finally keeping in mind the theory given above by Li et al. [12].

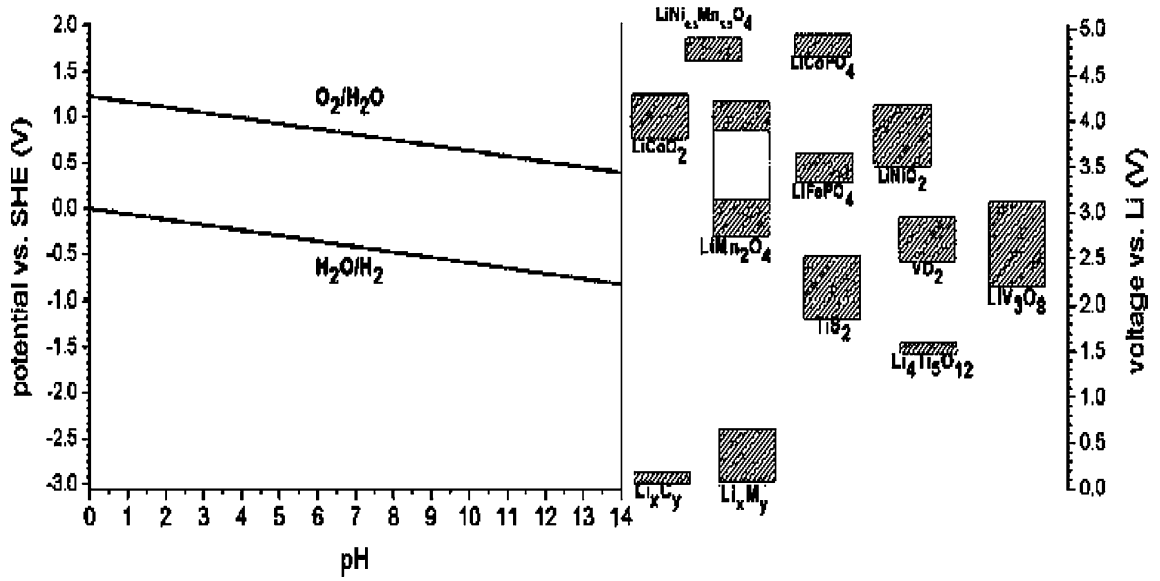

Fig. 2 Potential—pH diagram or Pourbaix diagram of various lithium intercalation compounds in aqueous solutions [38]

Lithium-ion kinetics

The lithium-ion transport kinetics is studied by assuming that lithium diffusion within the electrode is a rate-controlling step of the lithium intercalation process. During lithium transport, the unwanted reduction and oxidation of water may occur changing the pH of the electrolyte. However, aqueous lithium electrode materials are operated well within their water stability window. Thus the reduction and oxidation of water does not crucially influence the lithium transport kinetics of the electrode. Cell-impedance-controlled lithium transport mechanism was proposed by Lee and Pyun [14]. The AC impedance spectrum in aqueous electrolytes show only one semicircle in the high frequency region which corresponds to the charge transfer reaction unlike two semicircles observed in non-aqueous electrolytes. The surface film is not formed in aqueous electrolyte and charge transfer resistance is lowered by one order of magnitude compared to that in non-aqueous systems. This can be explained as follows. In aqueous electrolytes, the bare electrode is exposed to the electrolyte in the absence of surface layer and the charge transfer occurs easily across the electrolyte/electrode interface without the impeding effect of the surface layer. Both the high conductivity of aqueous electrolyte and the fast charge transfer kinetics are the main causes for the decreased R_{cell} in aqueous rechargeable lithium cells [15, 16]. Nakayama et al. [17] calculated the activation energy for the interfacial lithium-ion transfer reaction at the $LiMn_2O_4$ thin film electrode/aqueous solution and in organic electrolytes using the formula,

$$T/R_{ct} = A \exp^{(-Ea/RT)} \quad (7)$$

Where

E_a = the activation energy
T = the absolute temperature
R = gas constant
R_{ct} = the interfacial lithium-ion transfer resistance
A = the pre-exponential factor

The interfacial Li-ion transfer resistance estimated from the diameter of the semicircular arc of EIS was found to be 400 Ω in organic electrolytes and that reduced to 20 Ω in aqueous electrolyte. Activation energy calculated in 1 M $LiNO_3$ was 24 kJ mol^{-1}. However, it was 50 kJ mol^{-1} in organic electrolyte. Thus smaller activation energy of the aqueous system tends to enhance the interfacial lithium-ion transfer reaction rate.

The rate capability of charge–discharge process of the cell strongly depends on the charge transfer reaction step. According to Bruce and Saidi [18], an adsorption phenomenon is found at the electrode surface [18, 19]. The state of electrode surface affects the kinetics of the charge transfer reaction. Very recently Nakayama et al. have found that the presence of copper (II) ions [20] is found to retards the rate of charge transfer reaction by increasing the resistance of the lithium transfer process. Adsorption of Cu (II) ions on to the surface of the electrode will influence the interaction between hydrated lithium ions and the electrode surface. This indicates that Cu (II) ions should be completely removed from the electrolyte in practical aqueous rechargeable lithium batteries to enhance their rate capability.

Advantages and challenges with the use of aqueous electrolytes

Aqueous electrolytes have several advantages. Some of them are listed below.

a. They have high ionic conductivities so that thick electrodes can be used.
b. Expensive lithium salts like $LiPF_6$ can be replaced by cheap salts like $LiNO_3$, Li_2SO_4.
c. Costly separators can be replaced by inexpensive separators.
d. The safety issue is almost settled and strict cell assembly techniques are not required.

Aqueous rechargeable lithium batteries suffer from the following disadvantages.

(a) Cell potentials are restricted to the decomposition potential of water. Normally it is about 1.23 V which results in decreased energy density compared to non-aqueous electrolytes (>3.5 V)
(b) Poor cycling performances (about 25 cycles) which results in poor rate capability.

The various rechargeable lithium battery systems studied in aqueous electrolytes so far are listed in Table 1 and their properties are summarized.

Positive electrode materials

$LiMn_2O_4$ spinel

Table 2 summarizes the behavior of various cathode materials. Among many manganese oxide materials, spinel $LiMn_2O_4$ proposed by Thackery [21] has been attractive as cathode material. It has a cubic spinel structure that is closely related to α—$NaFeO_2$ layer structure with a cubic close packed oxygen array of anions. Manganese cations occupy half of the octahedral interstitial sites and Li^+ will occupy one eighth of tetrahedral sites. Mn_2O_4 framework provides three-dimensional interstitial space for Li^+ ion transport maintaining its structure over the compositional

Table 1 Overall summary of the cell performances of various rechargeable lithium battery systems in aqueous electrolytes

System	Electrolyte	Energy density (Wh/kg)	Maximum number of cycles	Average output voltage (V)	Reference
VO_2 (B)/$LiMn_2O_4$	5 M $LiNO_3$	55 (1)	20	1.5 8	8
$Li_2Mn_2O_9$/$LiMn_2O_4$	6 M $LiNO_3$	110 (1)	—	1.1	71
$Li_4Mn_5O_{12}$/$LiMn_2O_4$	6 M $LiNO_3$	110 (1)	—	1.1	71
LiV_3O_8/$LiMn_2O_4$	2 M Li_2SO_4	64.2 (1)	400	1.04	64
V_2O_5 xerogel/$LiMn_2O_4$	sat. $LiNO_3$	69 (1)	100	1.0	68
LiV_3O_8/$LiNi_{0.8}Co_{0.09}O_2$	1 M Li_2SO_4	30–60 (30)	100	1.5	63
$LiTi_2(PO_4)_3$/$LiMn_2O_4$	5 M $LiNO_3$	67.5 (1)	25	1.5	74
TiP_2O_7/$LiMn_2O_4$	5 M $LiNO_3$	58.8 (5)	25	1.4	74
$LiTi_2(PO_4)_3$/$LiMn_{0.05}Ni_{0.05}Fe_{0.9}PO_4$	sat. Li_2SO_4	78.3 (1)	50	0.9	76
PPy/$LiCoO_2$	sat. Li_2SO_4	40 (1)	120	0.85	77
$Li_xV_2O_5$-PPy/$LiMn_2O_4$	5 M $LiNO_3$	49.4 (1)	60	1.15	66
$Li_xV_2O_5$-PANI/$LiMn_2O_4$	5 M $LiNO_3$	51.7 (1)	120	1.1	67
LiV_3O_8/$LiCoO_2$	sat. $LiNO_3$	57.7 (1)	100	1.05	36
Zn/TiS_2-MnO_2	sat. LiOH + 1 M $ZnSO_4$	360 (1)	—	1.5	45, 46
Zn/TiB_2-MnO_2	– ” –	310 (1)	—	1.5	48
Zn/Bi_2O_3-MnO_2	– ” –	195 (1)	—	1.5	49
Zn/CeO_2-MnO_2	– ” –	232 (1)	10	1.5	51, 52
Zn/$LiMnPO_4$	– ” –	75 (1)	20	1.0	61

range $Li_xMnO_4 (0 \leq x \leq 1)$ by changing the average Mn oxidation state between 3.5 and 4.0. Dahn and coworkers in 1994, first time used $LiMn_2O_4$ as cathode material to construct an aqueous rechargeable cell [8]. However, in 1998, Weiss et al. [22] rejected the possibility of Li insertion into another host lattice ($YBa_2Cu_3O_7$) from saturated solutions of $LiNO_3$ though Dahn and coworkers confirmed it [10]. Proton insertion in $LiMn_2O_4$ when cycled in KOH media is reported [23]. Cyclic voltammetry and charge–discharge properties of undoped and Bi-doped $LiMn_2O_4$ in the 9 M KOH electrolyte revealed that Bi-doped spinels exhibit improved rechargeability. Lithium intercalation from the LiOH solution to form $Li_2Mn_2O_4$ from the host material of $LiMn_2O_4$ is described [14]. Recently Vivier et al. [24] reported the reversible proton insertion in $LiMn_2O_4$ from borate solutions. Li salt concentration in the electrolyte, type of electrolyte, and host lattice structure play a significant role on the electrochemical behavior of MnO_2 polymorphs [25]. Figure 3a shows the cyclic voltammogram of spinel $LiMn_2O_4$ in neutral saturated $LiNO_3$. This shows the presence of three cathodic peaks at 943, 804, and −377 mV vs SCE, three main anodic peaks at −121, 837 and 962 mV and a small anodic peak at 110 mV which represents the redox reaction of $LiMn_2O_4$/$Li_2Mn_2O_4$. Figure 3b shows the cyclic voltammograms of spinel $LiMn_2O_4$ in 1 M $LiNO_3$ which shows a depressed low potential peak at 110 mV. It is very clear from the figures that the peak corresponding to the reduction/oxidation of $LiMn_2O_4$ strongly depends on Li^+ concentration in the

Table 2 Electrochemical properties of cathode materials with different lithium intercalation compounds

Material	Electrolyte solution	Theoretical capacity (mAh/g)	Capacity in first cycle (mAh/g)	Capacity in *n* cycle(s) (mAh/g)	Current density/C_{rate}	Reference
$LiMn_2O_4$	1 M Li_2SO_4	148	84.6	50.1 (1,000)	0.1 Ag^{-1}	30
$LiMn_2O_4$/MWCNTs	1 M Li_2SO_4	148	117	112.8 (1,000)	0.1 Ag^{-1}	30
Submicron-sized $LiMn_2O_4$	5 M $LiNO_3$	148	73	——	C/1.5	28
$LiCoO_2$	5 M $LiNO_3$	140	112	105 (90)	1C	38
$LiMnO_2$	1 M Li_2SO_4		62	50 (150)	4.6 Ag^{-1}	32
γ-MnO_2	sat. LiOH + 1 M $ZnSO_4$	148	120	——	0.5 mA/cm^2	41
$LiMnPO_4$	LiOH+$ZnSO_4$	170	75	26 (20)	0.25 mA/cm^2	61
$LiMn_{0.05}Ni_{0.05}Fe_{0.9}PO4$	Li_2SO_4	170	87	55 (50)	0.2 mA/cm^2	76

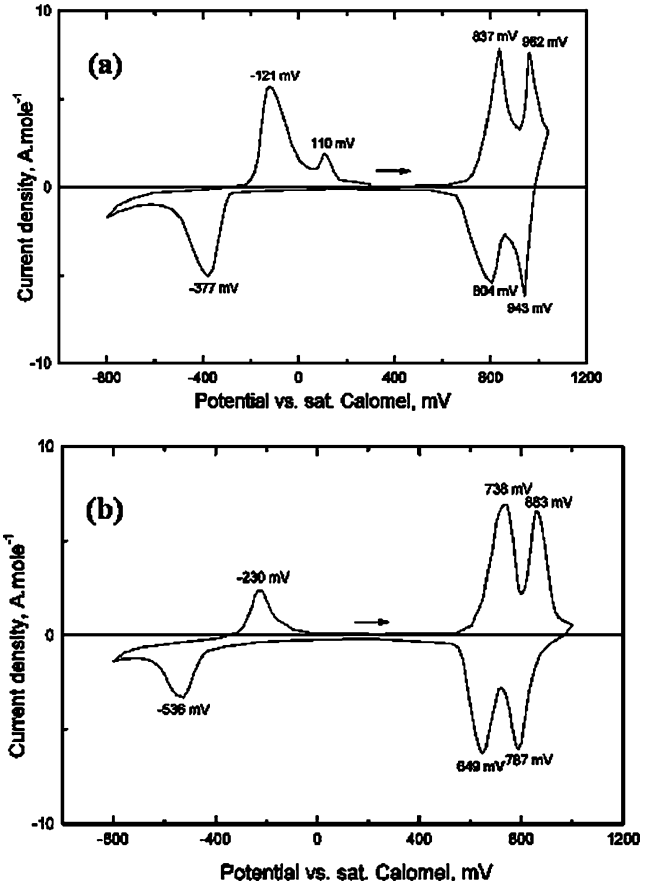

Fig. 3 **a** Cyclic voltammetry curve of $LiMn_2O_4$ in sat. $LiNO_3$. **b** Cyclic voltammetry in 1 M $LiNO_3$ [25]

electrolyte. The manganese oxides like spinel $LiMn_2O_4$ and γ-MnO_2 with three-dimensional framework of face sharing tetrahedral and octahedral for lithium diffusion are stable during lithium insertion/extraction. However, in saturated alkali nitrate electrolytes ($NaNO_3$ and KNO_3) only a small anodic peak appeared in the first oxidation step and it disappeared in the subsequent oxidation steps as shown in Fig. 4 a, b. Jayalakshmi et al. [26] reported a dual cation insertion/extraction into $LiMn_2O_4$ from different neutral aqueous electrolytes like LiCl, KCl, and NH_4Cl. For the first time they reported K^+ ion insertion into $LiMn_2O_4$. Proton insertion occurs at the neutral pH of these solutions along with Li^+, K^+, and NH_4^+. The presence of K^+ and NH_4^+ ions are found to ease the proton insertion/extraction reaction when compared to that of Li^+. The electrochemical behavior of $LiMn_2O_4$ materials of 400, 230, and 150 nm nanotubular diameters (outer diameter, OD) [27] in aqueous saturated $LiNO_3$ electrolyte revealed that the poor cycle performance is found to depend on thickness of the tubular wall of the electrode material and the unwanted oxidation of water during charging. The capacity of the electrode with smallest wall thickness (150 nm OD) is highest and it decreases as the thickness of the tubular wall increases. An experimental capacity of 104 mA hg^{-1} was obtained which may be compared with theoretical capacity of 148 mA hg^{-1} for $LiMn_2O_4$ at this 4 V plateau. This proves the better rate capability of nanostructured $LiMn_2O_4$ electrodes over conventional electrodes. At both high and low C_{rates}, a fraction of the current passed during charging is diverted to water oxidation rather than the desired Li^+ extraction process. The two horizontal lines in the Fig. 5a, b indicate the potential window where Li^+ extraction is the dominant reaction between 4.08 and 4.38 V. The coulombic efficiency at the optimum C_{rates} is highest for the 150 nm OD tubule electrodes and lowest for the 400 nm OD tubule electrodes. By controlling the charging rate (C_{rate}), so that it remains within the optimal potential window for Li^+ extraction from 4.08 to 4.38 V, the unwanted oxidation of water can be prevented which results in improved cycle performance. Submicron-sized particles of $LiMn_2O_4$ [28] exhibits high rate capability of 7 C in 5 M $LiNO_3$ aqueous electrolytes and shows only a slight decrease in the discharge capacity from 73 mA hg^{-1} (at C/1.5 rate) to 50 mA hg^{-1}. The discharge capacity of thin film $LiMn_2O_4$ [29] at a potential scan rate of 5 mV s^{-1} shows capacity loss

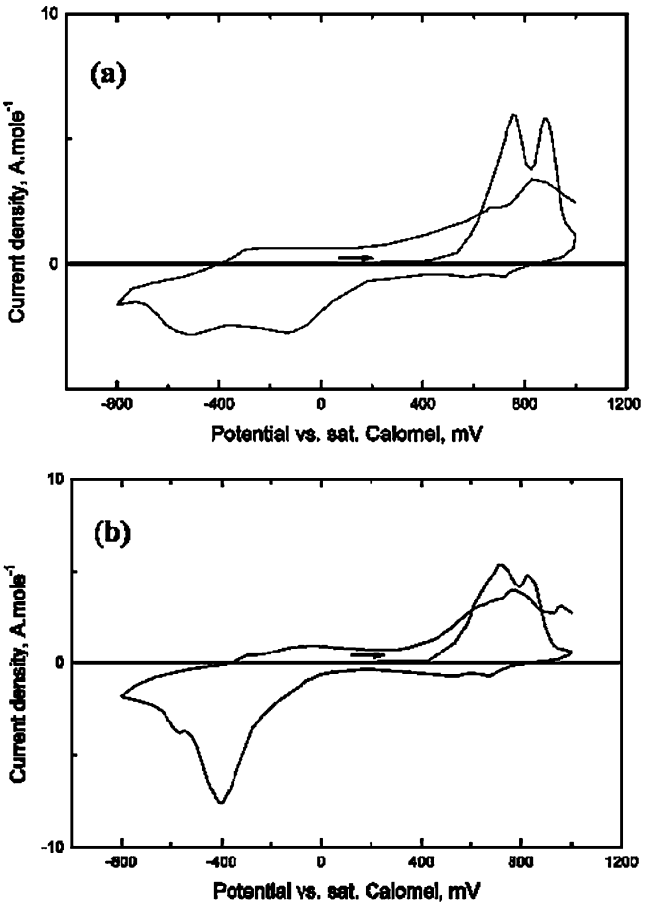

Fig. 4 Cyclic voltammetry curve of $LiMn_2O_4$ in, **a** sat. $NaNO_3$, **b** sat. KNO_3 [25]

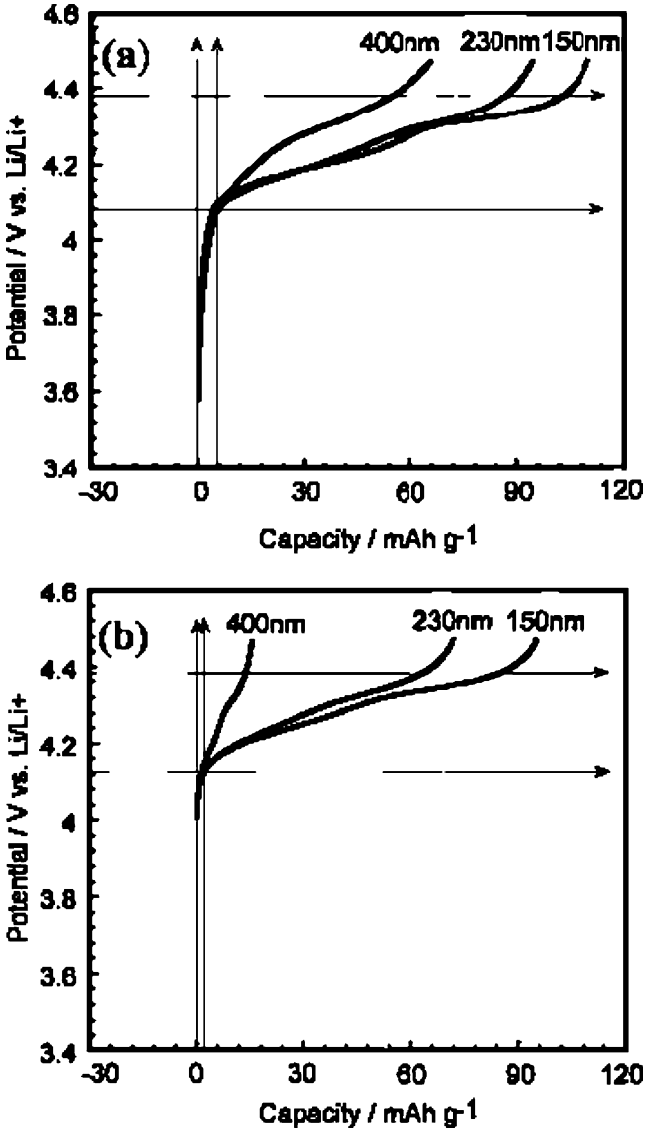

Fig. 5 **a** Charge curves for the three nanostructured electrodes at the lowest C_{rates} 400 (9 C), 230 (10 C), and 150 nm (11 C). The area between the *two horizontal lines* corresponds to the potential window for Li^+ extraction from $LiMn_2O_4$. The area between the *two vertical lines* corresponds to the amount of capacity that supports water oxidation in the low potential region. **b** Corresponding charging curves at the higher C_{rates} employed: 400 (92 C), 230 (97 C), and 150 nm (109 C) [27]

after 100 cycles was less than 10% indicating thin film electrode material is stable during lithium-ion extraction/insertion. Chen et al. [30] reported an improved electrochemical performance of $LiMn_2O_4$ when coated with MWCNTs. $LiMn_2O_4$/MWCNTs composite electrode maintained the discharge capacity of 112.8 mA hg^{-1} up to 1,000 cycles which is a good rate capability and cycling performance as shown in Fig. 6a, b. Electrochemical lithium insertion and extraction in Zn–Mn spinels like $ZnMn_2O_4$, $Zn_{0.5}Mn_2O_4$, and $Zn_yMn_{3-y}O_4+Mn_2O_3$ has also been reported from aqueous LiOH solutions [31]. The capacity obtained was above 200 mA hg^{-1} and cycling performance was very much influenced by the deep discharge process.

Layered oxides

Wu and Lee [32] have reported the fabrication of nanostructured manganese oxide on a stainless steel current collector by electrochemical, anodic deposition method. The electrode deposited at a high current density of 0.125 mA cm^{-2} and annealed at 300 °C is found to deliver maximum specific capacity of 62 mA hg^{-1} at a discharge current density of 4.6 Ag^{-1} in a high rate charge–discharge processes. Lithium deficient $Li_{1-x}NiO_2$ undergoes proton intercalation electrochemistry in aqueous solutions due to the strong hydration of lithium ions and the large size of the hydrated ions [33]. The electrochemical behavior of $LiCoO_2$ has been investigated in aqueous

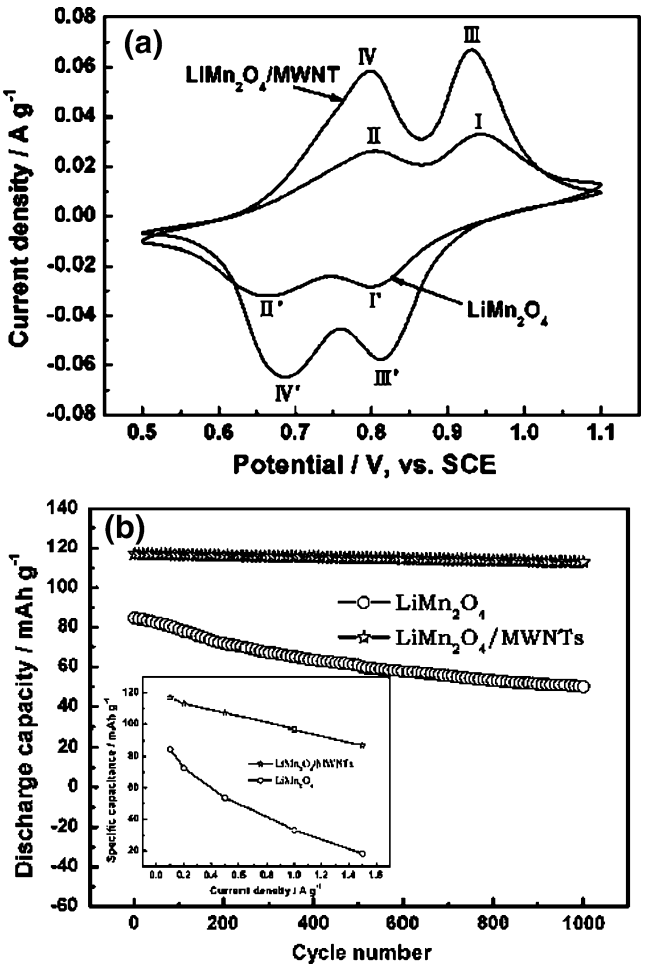

Fig. 6 **a** The CV curves of $LiMn_2O_4$ and $LiMn_2O_4$/MWNTs at a scan rate of 1 mV s^{-1}. **b** The cycling performance of $LiMn_2O_4$ and $LiMn_2O_4$/MWNTs at 0.1 A g^{-1}. The inset shows the discharge capacity of $LiMn_2O_4$ and $LiMn_2O_4$/MWCNTs at various current densities in 1 M Li_2SO_4 solution [30]

systems [34–39]. Figure 7a shows the cyclic voltammogram of $LiCoO_2$ in saturated $LiNO_3$. There is a significant decrease in the discharge capacity of the electrode material from its initial value of 60 mA hg^{-1} at a current density of 0.2 mA cm^{-2} to 40 mA hg^{-1} after 12 cycles in aqueous $LiNO_3$ electrolyte [37]. In another work, the initial value was 35 mA hg^{-1} at 1 C_{rate} and it falls significantly upon cycling to 20 mA hg^{-1} after 100 cycles [36]. An impressive kinetics and better cycle performance is observed when $Li_{0.5}Mn_2O_4$ is used as counter electrode [38] and is found to be crucial in the cycle performance of $LiCoO_2$ electrode material as it allows the cell to cycle reversibly compared to other counter electrodes like stainless steel, nickel mesh or Pt foil which are hardly inert or not fully reversible. The results obtained with this cell hardly changed even after 90 cycles as shown in Fig. 7b. Wang et al. [39] have demonstrated the electrochemical behavior of $LiCoO_2$ with spherical shape in saturated Li_2SO_4 solution using cyclic voltammetry and electrochemical impedance measurement techniques and compared the results with that in organic electrolytes. The electrode polarization occurs to a little extent in aqueous electrolytes unlike in organic electrolytes suggesting the high ionic conductivity of aqueous electrolytes playing significant role in the redox reactions of $LiCoO_2$ to get high rate capability and good reversibility

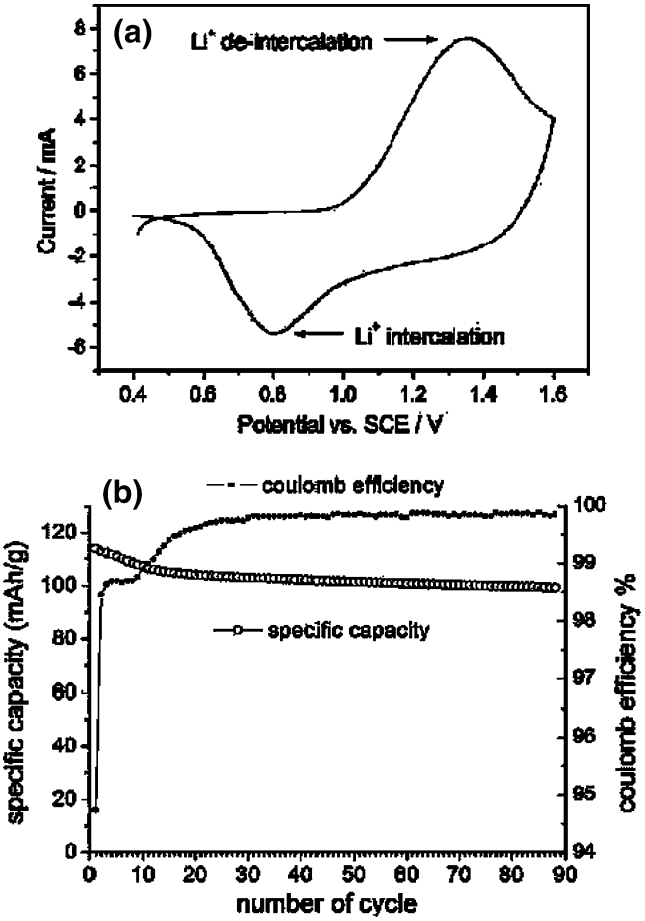

Fig. 7 **a** Cyclic voltammogram of $LiCoO_2$ in saturated $LiNO_3$ aqueous electrolyte with a scanning rate of 2 mVs^{-1} [39]. **b** Capacity vs number of cycles at 1 C_{rates} [38]

Manganese oxides

The first successful use of MnO_2 as a cathode material in aqueous rechargeable lithium battery was demonstrated by Deutscher et al. [40] in 1995. However the information was very limited. Later in 2004, Minakshi and coworkers [41–43] reported the electrochemical lithium insertion into manganese dioxide electrode in Zn/MnO_2 aqueous battery. In aqueous KOH electrolytes, the products formed upon discharging Zn/MnO_2 cell are MnOOH, Mn_2O_3 or Mn_3O_4.

$$\gamma - MnO_2 + xH^+ + xe- \rightarrow MnO_{2-x}(OH)_x \text{ For } X > 1 - Y - Z \quad (8)$$

$$Mn_{(1-Y)}O_{(1-3Y)}OH_{(1+3Y)} + xH^+ + xe- \rightarrow \text{Mixture of } \left[(Mn_2O_3 \text{ or } Mn_3O_4) + Mn(OH)_2\right] \quad (9)$$

These products are electrochemically irreversible which restricted its applications only to primary batteries. However in presence of LiOH aqueous electrolyte, the cell behavior is quite different and instead of H^+ insertion, Li^+ insertion occurs. The discharge curves were studied using two cells, one with KOH and another with LiOH as electrolytes. The cathode utilization in KOH cell was 41 % (120 mA hg^{-1}) as compared to 56% (162 mA hg^{-1}) for the LiOH cell. The discharge capacity for LiOH cell was higher. The calculated voltaic efficiency is 83% and this indicates that the cell can be reversibly discharged and charged. The difference in the reduction reaction of γ-MnO_2 in KOH and LiOH can be explained by considering the ionic sizes of K^+ and Li^+ ions [43]. The tunnel structures of γ-MnO_2 with rectangular-shaped cross sections will accept an ion whose ionic size is approximately equal to the size of Mn^{4+}. The ionic size of Li^+ is approximately same as that of Mn^{4+}, the coulombic interactions dominate and hence lithium intercalation/deintercalation takes place in LiOH solutions. However, the ionic size of K^+ is twice that of Li^+ and the insertion site is not stable as the electrostatic energy diminishes ruling out

K^+ intercalation into γ-MnO_2 to form K_xMnO_2. The XRD investigations of the cathode material after electrochemical lithium intercalation shows peaks (of lithiated Li_xMnO_2) that correspond to those reported for non-aqueous lithium cells by Aurbach and coworkers [44]. The cell voltage with battery grade manganese dioxide (BGM) is higher and it discharges at a higher voltage under identical conditions (current density, 0.5 mA cm^{-2}). It shows a sharp drop in voltage when the discharge capacity reaches 165 mA hg^{-1}. This different behavior of BMG compared to EMD may be due to a difference in the composition of two MnO_2 materials with respect to ramsdellite and pyrolusite, water content, and surface area [42].

Effect of additives on the electrochemical performance of γ-MnO_2

Addition of additives to MnO_2 slightly increases the battery performance. The effect of several additives on the performance of MnO_2 is summarized in Table 3. Addition of Ti^{4+} to MnO_2 cathode material and the cycle performance was studied in aqueous LiOH electrolyte [45, 46]. The improvement in the discharge capacity of the MnO_2 containing TiS_2 additive between 1 and 3 wt% was due to the stabilizing effect of TiS_2 towards dimensional changes that occur during the discharge process [47]. When the additive content was increased from 3 to 5 wt%, a coating of nanoparticulate Mn oxyhydroxides is found to form on the electrode inhibiting lithium intercalation and accounts for the low battery performance of MnO_2. TiB_2 is found to suppress the formation of unwanted discharge products such as birnessite (δ-MnO_2) and hausmannite (Mn_3O_4) and facilitates formation of more lithiated MnO_2. It stabilizes the structure of MnO_2 after discharge and prevents the dissolution of Mn^{3+} ions from the solid [48]. When the concentration of TiB_2 in MnO_2 cathode is above 3 wt%, the stabilizing effect on the structure of MnO_2 containing edge-shared MnO_2 octahedra is reversed. This offers a resistance to the ionic migration of Li in and out of the lattice decreasing the capacity of the cell to 100 mA hg^{-1}. The addition of Bi_2O_3 into MnO_2 [49] significantly increases the cycle performance. Unlike for Ti additives, the radius of Bi (III) is very large (0.93 Å) compared with Mn (III) (0.73 Å) and also bismuth can interact with any amount of manganese due to its strong interactions with manganese [50]. This tendency of bismuth to interact strongly with manganese will prevent the formation of unwanted, irreversible products like birnessite, hausmannite and oxyhydroxy phase which are well known to decrease the cell capacity. Recently the cerium oxide (CeO_2) modified MnO_2 cathode that offer an improved discharge capacity has been reported [51, 52]. The optimum concentration of CeO_2 in the cathode at which the cell delivers maximum capacity is found to be 2 wt%. The interesting thing is that its effect on the cycle performance of MnO_2 cathode is observed from the second cycle during discharge. XRD, TEM, EELS and IR spectral investigations of the cathode material after the first discharge and subsequent charge–discharge cycles revealed that after the first discharge manganese gets reduced to various oxides and hydroxides (Mn_2O_3, MnOOH and MnO) along with the formation of lithiated manganese oxide (Li_xMnO_2). However mid-infrared spectral studies show that the peaks corresponding to the formation of Mn_2O_3, MnOOH and MnO diminished from second discharge and these products are not formed. This clearly accounts for the low capacity during the first cycle and increased capacity after second and subsequent cycles of CeO_2 modified cell. Figure 8 shows the effect of these additives on the electrochemical performance of MnO_2.

Anatase TiO_2

The semiconducting properties of TiO_2 together with its chemical stability make it an excellent candidate as cathode material for rechargeable lithium batteries. The anatase form of TiO_2 was found to intercalate Li^+ ions from non-aqueous electrolytes than its rutile form due to difference in their structures. Anatase TiO_2 undergoes reduction through more than one mechanism forming four different reduction products, Li_xTiO_2, Ti_2O_3, Ti_2O and TiO [53]. Out of these four reduction products only Li_xTiO_2 undergoes reversible oxidation.

Table 3 Effect of additives on the cycle performance of γ-MnO_2 cathode in Zn/LiOH/MnO_2 cell

Additive	Optimized percentage of the additive	Discharge capacity (m Ah g^{-1})		Reference
		Without additive	With additive	
TiS_2	3 wt%	140	240	45, 46
TiB_2	1 wt%	150	200	48
Bi_2O_3	6 wt%	148 (1 cycle) 70 (40th cycle)	130 (50th cycle)	49
CeO_2	2 wt%	148	155 (1 cycle) 190 (from 2 cycle)	51, 52

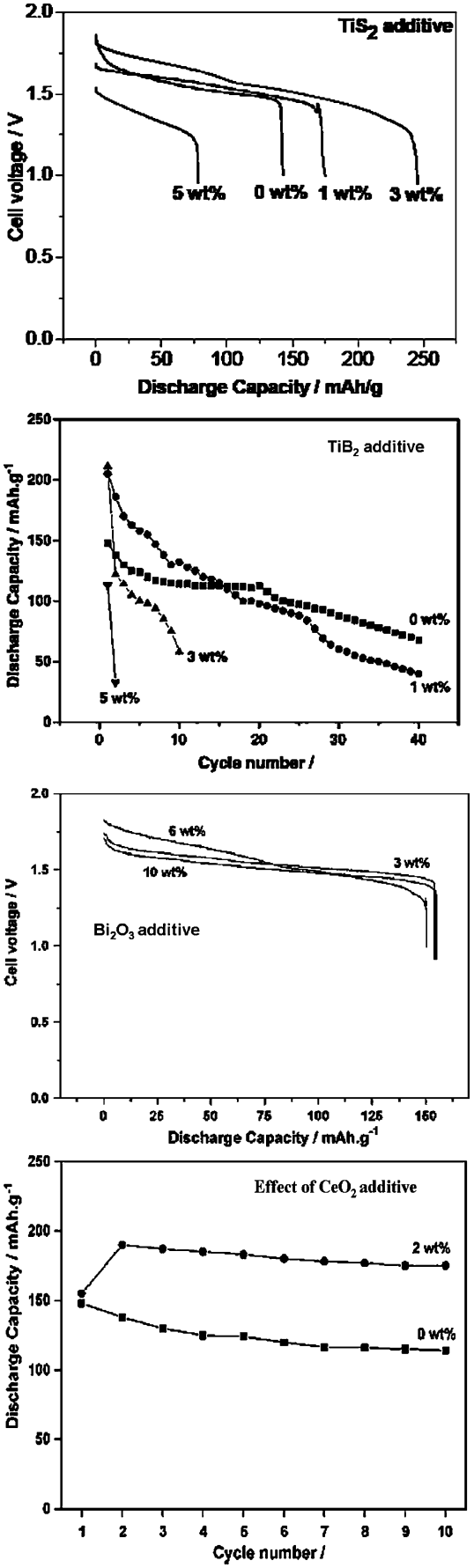

◀ **Fig. 8** Effect of various additives on the electrochemical performance of γ-MnO_2 phase [46, 48, 49, 51, respectively]

Olivine compounds

The presence of $(PO_4)^{3-}$ polyanions with a strong P-O covalent bond in olivine structure provides stable system when the electrode is fully charged [54]. Main drawback of the material is its low electrical conductivity [55, 56] and small lithium-ion diffusivity. This can be improved by reducing the particle size and coating $LiFePO_4$ particles with a layer of carbon. In aqueous solutions, $LiFePO_4$ undergoes a partially reversible oxidation/reduction via lithium insertion/extraction mechanism due to the formation of $FePO_4$ during extraction process [57]. The reverse reduction of $FePO_4$ is not fully reversible as it forms a mixture of $LiFePO_4$ and Fe_2O_3. This leads to a decrease in the Li/Fe ratio and causes capacity loss from second and fifth cycle. Mi et al. [58] have shown that the redox behavior of $Li_{0.99}Nb_{0.001}FePO_4$ compound is influenced by the magnitude of scan rate. This behavior may arise from the transformation of one phase to another or due to a difference in the E^0 values of two distinct chemical species formed. Tarascon and coworkers [59] introduced the factors affecting the electrochemical reactivity of carbon-free $LiFePO_4$ thin films in aqueous and non-aqueous electrolytes and found that a lowering of both the cell resistance and interfacial charge transfer resistance in aqueous electrolytes increased the capacity of $LiFePO_4$ thin films. Very recently Liu et al. [60] have found modifying $LiFePO_4$ with CeO_2 provides a good electrical contact between oxides. The cyclic voltammetry study strongly suggested that CeO_2 modification improved the reversibility and D_{Li+} values.

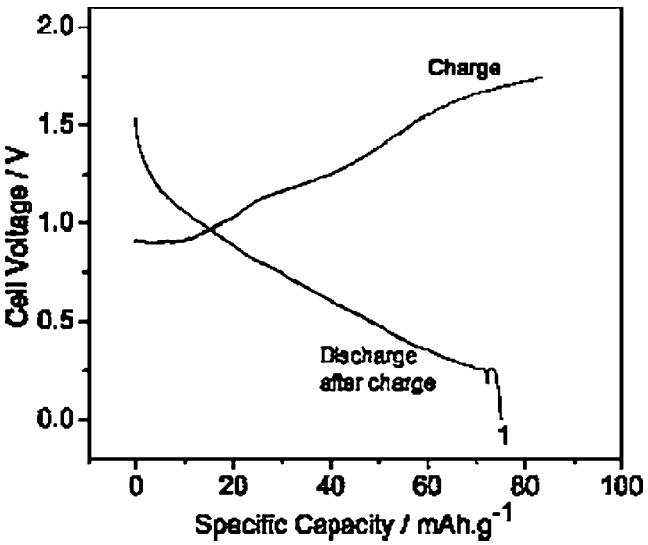

Fig. 9 First charge and discharge curve of Zn-$LiMnPO_4$ cells using saturated aqueous LiOH containing 1 mol L^{-1} of $ZnSO_4$ electrolyte [61]

The electrochemical behavior of $LiMnPO_4$ is slightly different than that of $LiFePO_4$ [61]. It undergoes electro-oxidation to form $MnPO_4$ and this reaction is reversible unlike $LiFePO_4$. Figure 9 shows the galvanostatic charge–discharge curves obtained with the cell, Zn/LiOH+$ZnSO_4$/$LiMnPO_4$. There is slight inflection around 1.1 and 1.5 V during charging which may be due to twinning effect caused by the delithiation in olivine structure. However, this inflection was not observed during discharge.

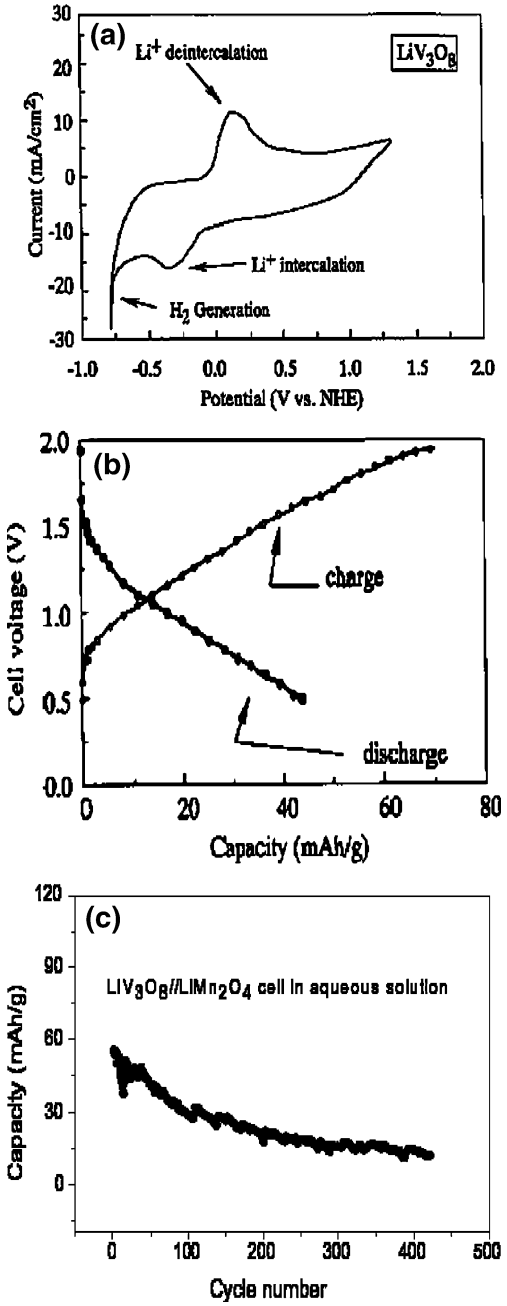

Fig. 10 **a** Cyclic voltammogram of LiV_3O_8 in 1 M-Li_2SO_4 aqueous electrolyte with a scanning rate of 20 mVs^{-1} vs Ag/AgCl [63]. **b** Charge–discharge curves of a $LiNi_{0.81}Co_{0.19}O_2$/1 M-Li_2SO_4 soln/LiV_3O_8 cell in a 1.9-V charge experiment [63]. **c** Cycling performance of the LiV_3O_8/$LiMn_2O_4$ cell at a current rate of 0.2 C between 0.5 and 1.5 V [64]

Negative electrode materials

Vanadium oxides

Dahn and group [11] used VO_2 (B) as anode material to insert lithium ions on charging and this process is reversible. But it suffers from capacity loss (around 17 cycles).

C/VO_2 (B) core shell micro sphere exhibits [62] improved cycle performance in aqueous 2 M LiCl even after 80 cycles compared to that of pure VO_2 (B).The rigid core/shell nanostructure of C/VO_2 (B) is responsible for the improved cycling performance which can avoid the aggregation of active materials during a long cycling process and provide a large surface area and short diffusion distance. Kohler et al. [63] have characterized LiV_3O_8 as anode material for aqueous lithium batteries. Figure 10a shows the cyclic voltammogram of LiV_3O_8 in 1 M Li_2SO_4 and Fig. 10b shows the charge–discharge curves of the cell, $LiNi_{0.81}Co_{0.19}O_2$/1 M Li_2SO_4 sol/LiV_3O_8. The cell potential changes gradually during charging and discharging without formation of a plateau with a discharge capacity between 40 and 45 mA hg^{-1}. However, rapid fall in the performance of LiV_3O_8 at high potential of 1.9 V indicates that LiV_3O_8 is less stable in aqueous electrolytes. Electrode deterioration occurs due to the chemical reactions between the electrolyte and electrode. Wang et al. [64] have found a better cycle performance with a capacity retention of 29.5 and 20.2 mA hg^{-1} after 100 and 220 respectively. After 400 cycles, the discharge capacity was still above 10 mA hg^{-1} as shown in Fig. 10c. LiV_3O_8 has a very stable layered structure due to the pinch of function of the existing Li^+ cations between the layers of VO_6 octahedral and VO_5 trigonal bipyramids. Pristine LiV_3O_8 is reported [65] to undergo a three-stage intercalation reaction. Though it exhibits good cycling performance, there are side reactions causing the capacity fading. Recently polypyrrole (PPy) [66] and polyaniline (PANI) [67]-coated $Li_xV_2O_5$ electrode materials have been proposed as anode materials which stabilize the cycle performance of aqueous rechargeable lithium batteries. Figure 11a shows the discharge capacity of the aqueous cell with PPy along with coulombic efficiency and Fig. 11b shows cycling characteristics of cells made up of PANI-coated $Li_xV_2O_5$ anode materials. In case of PPy-coated $Li_xV_2O_5$ anode, the cell retained 86% of its initial discharge capacity after 40 cycles while the cell with bare anode retained only 8%. The cell delivered a capacity of 43 mA hg^{-1} at an average voltage of 1.15 V. In case of PANI-coated $Li_xV_2O_5$, the cell retained 80% of its initial capacity after 40 cycles while the cell with bare

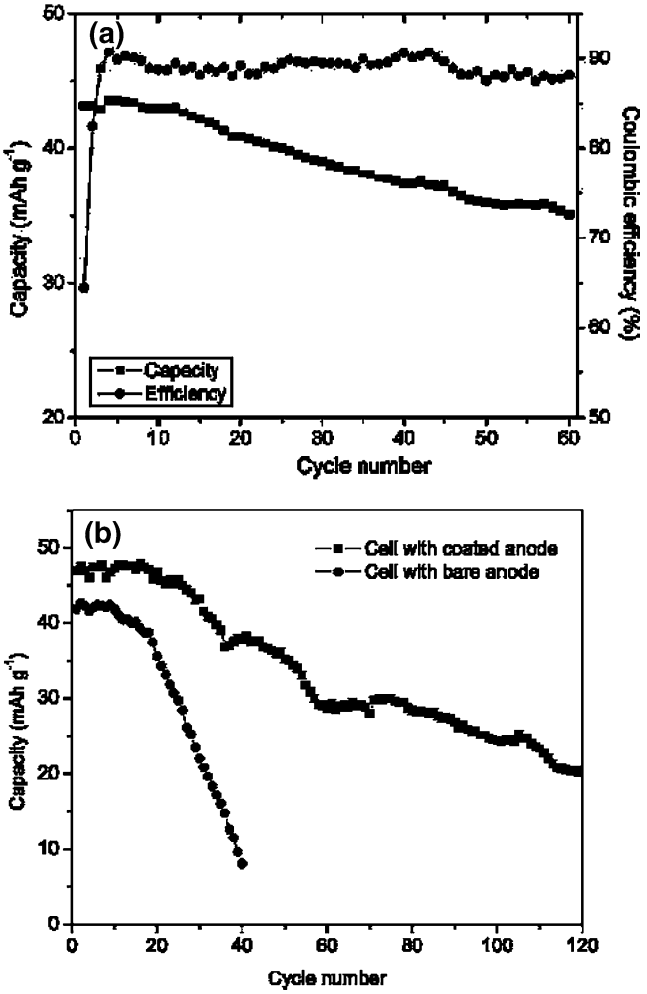

Fig. 11 **a** Cycling stability and coulombic efficiency curves of cells with bare anode and PPy-coated anode at 0.2 C_{rate} between 0.6 and 1.7 V [66]. **b** Cycling characteristics of cells with (*filled square*) PANI-coated and (*filled circle*) bare anode between 1.8 and 0.5 V at 0.2 C [67]

anode retained only 20% of initial capacity. The cell delivers a capacity of 47 mA hg^{-1} at an average voltage of 1.1 V. However, faradaic capacity of polymer coated $Li_xV_2O_5$ did not exceed beyond 50 mA hg^{-1} in both the cases. The presence of optimum water content of 0.3 mole per mole of V_2O_5 can deliver higher faradaic capacity and provide longest cycle life. Stojkovic et al. [68] have demonstrated the use of xerogel V_2O_5 ($V_2O_5{\cdot}nH_2O$) as anode material in aqueous saturated $LiNO_3$. The xerogel V_2O_5 contain sheets comprised of two vanadium oxide layers with all the vanadyl bonds on the outside leading to a distorted octahedral structure around the lithium instead of the square pyramidal structure found in crystalline V_2O_5 [69, 70]. The galvanostatic charge–discharge profiles of cell, xerogel V_2O_5/sat. $LiNO_3$/$LiMn_2O_4$ shows only about 11% capacity fading after 100 cycles which is a better performance compared to that of crystalline V_2O_5 electrodes [66, 67]. The capacity fade was most pronounced in the first 30 cycles and became negligible afterwards.

Li-Mn spinels

$Li_2Mn_4O_9$ and $LiMn_5O_{12}$ have a defect spinel–framework structure that can be represented as $[Li_{0.89}]_{8a}$ $[Mn_{1.78}]_{16d}$ $[O_4]_{32e}$ and $[Li_{0.89}]_{8a}$ $[Li_{0.33}Mn_{1.66}]_{16d}$ $[O_4]$ respectively. This structure provides a three-dimensional tunnel for Li^+ insertion and extraction with least change in the unit cell volume. These materials can accommodate three Li ions per formula and the ideal reactions of cells $Li_2Mn_4O_9$/$LiMn_2O_4$ and $LiMn_2O_4$/$Li_4Mn_5O_{12}$ are,

$$Li_5Mn_4O_9 + Mn_2O_4 \rightleftarrows Li_2Mn_4O_9 + 3LiMn_2O_4 \quad (10)$$

$$Li_7Mn_5O_{12} + Mn_2O_4 \rightleftarrows Li_4Mn_5O_{12} + 3LiMn_2O_4 \quad (11)$$

The cells constructed using these anode materials delivered a capacity of 100 mA hg^{-1} at an average voltage of 1–1.1 V [71]. $Li_4Ti_5O_{12}$ was also studied for a possible anode material with $LiMn_2O_4$ cathode. The cell was expected to deliver 2.4–2.5 V. To get this voltage, the cell should be charged beyond 2.0 V during first charging. This leads to failure of the cell due to H_2 evolution on $Li_4Ti_5O_{12}$ anode.

Nanostructured TiO_2

Reiman et al. [72] studied the electrochemical lithium insertion into TiO_2 from aqueous 1 M LiOH solution and confirmed the lithium ion insertion in spite of the parasitic hydrogen evolution reaction. A limiting composition of $Li_{0.27}TiO_2$ was obtained at a potential of −0.85 V vs RHE beyond which the hydrogen evolution caused a rapid self-

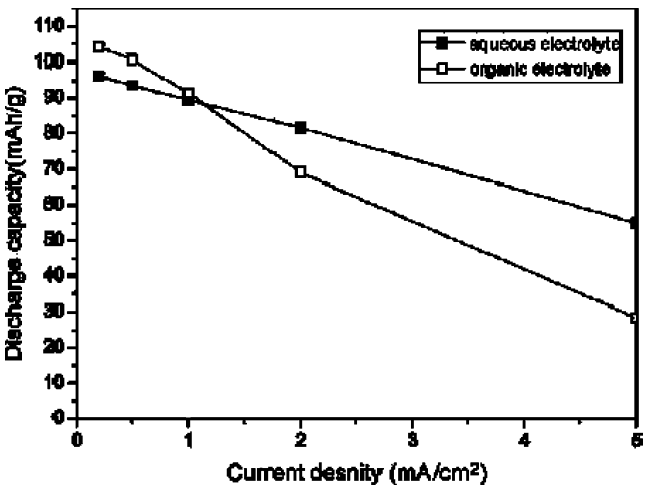

Fig. 12 Rate capabilities of $LiMn_{0.05}Ni_{0.05}Fe_{0.9}PO_4$/$LiTi_2(PO_4)_3$ with different electrolytes [76]

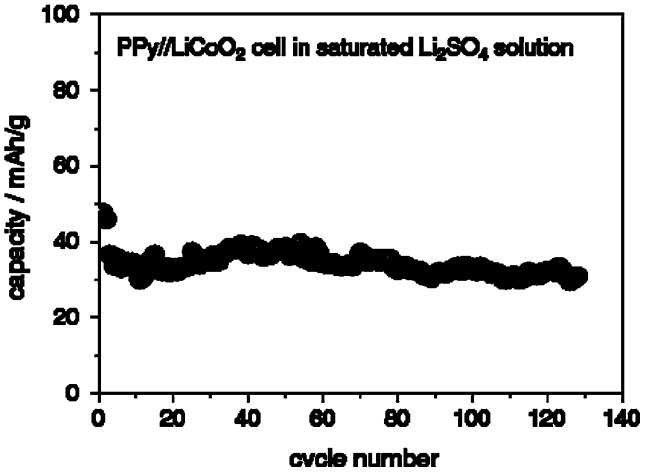

Fig. 13 Cycling behavior of the aqueous rechargeable lithium battery based on doping (PPy) and intercalation ($LiCoO_2$) compounds at 0.1 C_{rate} [77]

discharge. However, this work aimed at developing a nanostructured super capacitors with NiOOH as positive electrode and LiOH as the electrolyte. Recently Wu et al. [73] have reported the electrochemical performance of nanostructured anatase TiO_2 fabricated directly on to the stainless steel mesh using electrochemical anodic deposition strategy. The synthesized anatase TiO_2 films were subjected to annealing at different temperature and the influence of annealing temperature on the electrochemical performance of the anode material was also investigated. The optimum temperature at which anatase TiO_2 films exhibit good performance is 400 °C

NASICON-type and pyrophosphate compounds

Polyanionic compounds particularly phosphate-based compounds have attracted the interest of battery scientists as cathode materials in non-aqueous lithium batteries. Wang et al. [74] have reported the electrochemical behavior of pyrophosphates, TiP_2O_7 and NASICON-type $LiTi_2(PO_4)_3$ as anode materials in 5 M $LiNO_3$ aqueous electrolyte due to their lower Li-ion intercalation and deintercalation potentials so that they can fully use the stability window of aqueous electrolytes. The negative values of redox potentials of the materials suggest that they can be used as anode materials for aqueous rechargeable lithium battery. In case of TiP_2O_7 the hydrogen evolution peaks shifts below −0.60 V and in case of $LiTi_2(PO_4)_3$ it shifts below −0.70 V. This shift in hydrogen evolution peak confirm the over potential effects of these anode materials on hydrogen evolution reaction and they can use the full stable potential window of water in aqueous rechargeable batteries. $TiP_2O_7/LiMn_2O_4$ cell delivers a capacity of about 42 mA hg^{-1} at an average voltage of 1.4 V between 0.80 and 1.70 V and $LiTi_2(PO_4)_3/LiMn_2O_4$ delivers a capacity of 45 mA hg^{-1} at an average voltage of about 1.5 V between 0.90 and 1.85 V. Though the theoretical specific energies of $TiP_2O_7/LiMn_2O_4$ and $LiTi_2(PO_4)_3/LiMn_2O_4$ cells are 96.6 and 114.4 mW hg^{-1} respectively, achieving the theoretical capacities still remain a challenge to battery scientists. In another work, Luo et al. [75] have reported better electrochemical performance of $LiTi_2(PO_4)_3$ synthesized by chemical vapor deposition technology. The cell, $LiTi_2(PO_4)_3/LiMn_2O_4$ delivers capacity of 40 mA hg^{-1} and specific energy of 60 mW hg^{-1} in 1 M Li_2SO_4 solution with an output voltage of 1.5 V. Only about 18% of capacity fading was observed over 200 charge–discharge cycles which is much better battery systems studied in aqueous electrolytes. Recently, Liu et al. [76] have reported the electrochemical performance of $LiTi_2(PO_4)_3/LiMn_{0.05}Ni_{0.05}Fe_{0.9}PO_4$ in saturated aqueous Li_2SO_4 and compared its rate capabilities with that in organic electrolytes. As the current density is increased, the discharge capacity increased in aqueous electrolytes and decreased in organic

Table 4 Electrochemical properties of anode materials with different lithium intercalation compounds

Material	Electrolyte solution	Theoretical capacity (mAh/g)	Capacity in first cycle (mAh/g)	Capacity in *n* cycle(s) (mAh/g)	Current density/C_{rate}	Reference
VO_2 (B)		——	100			11
$Li_xV_2O_5$	5 M $LiNO_3$	75	40	5 (40)	0.2 C	66
$Li_xV_2O_5$/Ppy	5 M $LiNO_3$	75	47	45 (60)	0.2 C	66
$Li_xV_2O_5$/PANI	5 M $LiNO_3$	75	47	22 (120)	0.2 C	67
LiV_3O_8	1 M Li_2SO_4	145	40–45	10 (400)	1 mA/cm^2	63, 64
V_2O_5 xerogel	sat. $LiNO_3$	75	69	61 (100)	0.2 C	68
$Li_2Mn_4O_9$	6 M $LiNO_3$	156	110	——	1 mA/cm^2	71
$Li_4Mn_5O_{12}$	6 M $LiNO_3$	202	110	——	1 mA/cm^2	71
TiP_2O_7	5 M $LiNO_3$	——	100	80 (2)	——	74
$LiTi_2(PO_4)_3$	5 M $LiNO_3$	——	80	90 (2)	——	76
Polypyrrole (Ppy)	sat.Li_2SO_4	120	52.5	52 (120)		75

electrolytes as shown in Fig. 12. This shows the advantage with aqueous electrolytes. Thus aqueous electrolytes provide a promising mean of solving the low electrical conductivities of these NASICON-type anode materials.

Conducting polymers

Use of conducting polymer, polypyrrole as anode material has been demonstrated for the first time in aqueous electrolytes by Wang et al. [77]. The battery makes use of a new technique which solves the major problem of poor cycle performance of aqueous rechargeable lithium batteries known so far and provides a new strategy to explore advanced energy storage and conversion systems. The cell, PPy/$LiCoO_2$, exhibits a coulombic efficiency of 91.4%. The average charge–discharge voltages are 1.0 and 0.86 V with a capacity of 52.2 and 47.7 mA hg^{-1} respectively. Capacity fading was not observed during the first 120 cycles as evident from the Fig. 13. The advantages with this cell are doping/dedoping processes are highly reversible with PPy, the possible cycle numbers can be above 1,000 [78] and superior to vanadium oxide negative electrodes such as VO_2 and LiV_3O_8 and $LiCoO_2$ exhibits a very good cycling behavior in aqueous electrolytes [38].

Carbon and other anode materials

Carbon is well studied as anode material in non-aqueous medium since it is known to intercalate lithium from organic solvents [79]. However the use of carbon as an anode material in aqueous rechargeable lithium battery was reported to be impossible as it catalyzes the hydrogen evolution process in saturated LiCl/LiOH at potentials more negative than about −1.5 V. Molybdenum dioxide and ferric oxide electrodes could be used only in the potential window of −0.2 to −1.3 V. Among several metal anodes studied in aqueous LiCl/LiOH solutions in terms of charge recovery, mercury exhibits 85% charge recovery which is an ideal requirement for battery applications. However, it is not an ideal practical anode material. It forms amalgam with lithium reducing its activity. Aluminum and bismuth shows a charge recovery of 21% and 20%, respectively [40]. Table 4 summarizes the behavior of various anode materials

Conclusion and future directions

$LiMn_2O_4$ is found to be a good candidate as cathode material for aqueous rechargeable batteries due to its low cost compared to $LiCoO_2$ and other materials. When combined with MWCNTs, it exhibits good cycling performance as high as 1,000 cycles. Lithium metal phosphates and pyrophosphates are also attractive as cathode materials. Before commercialization of aqueous rechargeable lithium battery, further work is needed to improve the coulombic and voltaic efficiencies along with the cycle life of the materials. This may include increasing the energy density since lead-acid battery works at 2 V with aqueous electrolytes, understanding the competition between hydrogen and lithium insertion, effect of various additives like rare earth metal oxides, sulphides and oxides towards stabilizing the dimensional changes of the lattice structure and exploring the chemistry of LiCl as electrolyte. The reported capacity of these cells, so far, is too low for portable electronic devices and they may be of interest in stationary systems. The success of aqueous rechargeable lithium battery or any progress in this technology depends strongly on solid-state research or material science research which plays a crucial role in developing, improved new cathode or anode materials

Acknowledgment Financial support from the Department of Science and Technology, Government of India is greatly acknowledged. The authors wish to thank Sri. A. V. S. Murthy, honorary secretary, Rashtreeya Sikshana Samiti Trust, Bangalore and Dr. P. Yashoda, Principal, SSMRV Degree College, Bangalore for their continuous support and encouragement.

References

1. Pasquier AD, Plitz I, Menocal S, Amatucci G (2003) J Power Sources 115:171
2. Chau KT, Wong YS, Chan CC (1999) Energy Convers Manage 40:1021
3. Frost PC (1999) J Power Sources 78:256
4. Gifford P, Adams J, Corrigan D, Venkatesan S (1999) J Power Sources 80:157
5. Wade EJ (1902) Secondary batteries: the electrician, London. Van Nostrand, New York
6. Barak M (ed) (1980) Electrochemical power sources. Peter Peregrins, London
7. Wakihara M (2001) Mater Sci Eng Rep 33:109
8. Li W, Dahn JR, Wainwright DS (1994) Science 264:1115
9. Glanze J (1994) Science 264:1084
10. Li W, Dahn JR (1995) J Electrochem Soc 142:1742
11. Zhang M, Dahn JR (1996) J Electrochem Soc 143:2730
12. Li W, Mckinnon WR, Dahn JR (1994) J Electrochem Soc 141:2310
13. Mckinnon WR, Hearing RR (2007) In: White RE, Bockris J'O'M, Conway BE (eds) Modern aspects of electrochemistry. No.15. Plenum press, New York
14. Lee J-W, Pyun S-Il (2004) Electrochim Acta 49:753
15. Aurbach D, Gamolsky K, Markovsky B, Salitra G, Gofer Y, Heider U, Oesten R, Schmidt M (2000) J Electrochem Soc 147:1322
16. Zhang SS, Xu K, Jow TR (2002) J Electrochem Soc 149:A1521
17. Nakayama N, Nozaw T, Iriyama Y, Abe T, Ogumi Z, Kikuchi K (2007) J Power Sources 174:695
18. Bruce PG, Saidi MY (1992) J Electroanal Chem 322:93
19. Nakayama N, Nozawa T, Iriyama Y, Abe T, Ogumi Z, Kikuchi K (2007) J Power Sources 174:695

20. Nakayama N, Yamada I, Huang Y, Nozawa T, Iriyama Y, Abe T, Ogumi Z (2009) Electrochim Acta 54:3428
21. Thackery MM, David WIF, Bruce PG, Goodenough JB (1983) Mater Res Bull 18:461
22. Weiss M, Gunther W, Schollhorn R (1998) Phys C 304:156
23. Schlorb H, Bungs M, Plieth W (1997) Electrochim Acta 42:2619
24. Vivier CC, Bash S, Ramos JP (1999) Electrochim Acta 44:2705
25. Abou-El-Sherbini KS, Askar MH (2003) J Solid State Electrochem 7:435
26. Jayalakshmi M, Mohan Rao M, Scholz F (2003) Langmuir 19:8403
27. Li N, Patrissi CJ, Che G, Martin CR (2000) J Electrochem Soc 147:2044
28. Sinha NN, Ragupathy P, Vasan HN, Munichandraiah N (2008) Int J Electrochem Soc 3:691
29. Eftekhari A (2001) Electrochem Acta 47:495
30. Chen S, Mi C, Su L, Gao B, Fu Q, Zhang X (2009) J Appl Electrochem 39:943
31. Hui Y, Huaquan Y, Yinlin L, Neng L, Bingxiong L (1996) J Power Sources 62:223
32. Wu M-S, Lee R-H (2008) J Power Sources 176:363
33. Mohan Rao M, Jayalakshmi M, SchaÈ O, Guth U, Wulf H, Scholz F (1999) J Solid State Electrochem 4:17
34. Lee JH, Han KS, Lee BJ, Seo S, Yoshimura M (2004) Electrochim Acta 50:467
35. Wang YG, Luo JY, Wang CX, Xia YY (2006) J Electrochem Soc 153:A1425
36. Wang G, Fu L, Zhao N, Yang L, Wu Y, Wu H (2007) Angew Chem Int Ed 46:295
37. Wang GJ, Zhao NH, Yang LC, Wu YP, Wu HQ, Holze R (2007) Electrochim Acta 52:4911
38. Ruffo R, Wessels C, Huggins RA, Cui Y (2009) Electrochem Commun 11:247
39. Wang GJ, Qua QT, Wang B, Shi Y, Tian S, Wu YP, Holze R (2009) Electrochim Acta 54:1199
40. Deutscher RL, Florence TM, Woods R (1995) J Power Sources 55:41
41. Minakshi M, Singh P, Issa TB, Thurgate S, Marco RD (2004) J Power Sources 130:254
42. Minakshi M, Singh P, Issa TB, Thurgate S, Marco RD (2004) J Power Sources 138:319
43. Minakshi M, Singh P, Issa TB, Thurgate S, Marco RD (2006) J Power Sources 153:165
44. Levi E, Zingrad E, Teller H, Levi MD, Aurbach D, Mengeritsky E, Elster E, Dan P, Granot E, Yamin H (1997) J Electrochem Soc 144:4133
45. Minakshi M, Singh P, Mitchell DRG, Issa TB, Prince K (2007) Electrochim Acta 52:7007
46. Minakshi M, Mitchell D, Singh P, Thurgate S (2006) Australian Institute of Physics 17th National Congress 2006, Brisbane, page 3
47. Yao YF, Gupta N, Wroblowa HS (1987) J Electroanal Chem 223:107
48. Minakshi M, Mitchell DRG, Prince K (2008) Solid State Ion 179:355
49. Minakshi M, Mitchell DRG (2008) Electrochim Acta 53:6323
50. Qu DY (1999) J Appl Electrochem 29:511
51. Minakshi M, Mitchell DRG, Carter ML, Appadoo D, Nallathamby K (2009) Electrochim Acta 54:3244
52. Minakshi M, Nallathamby K, Mitchell DRG (2009) J Alloys Compds 479:87
53. Minakshi M, Singh P, Issa TB, Thurgate S (2006) J Appl Electrochem 36:599
54. Padhi AK, Nanjundaswamy KS, Goodenough JB (1997) J Electrochem Soc 144:1188
55. Jiang J, Dahn JR (2004) Electrochem Commn 6:39
56. Takahashi M, Tobishima SI, Takei K, Sakurai Y (2002) Solid State Ion 148:283
57. Minakshi M, Singh P, Thurgate S, Prince K (2006) J Power Sources 158:646
58. Mi CH, Zhang XG, Li HL (2007) J ElectroanalChem 602:245
59. Sauvage F, Laffont L, Tarascon JM, Baudrine E (2008) J Power Sources 175:495
60. Liu Y, Mi C, Yuan C, Zhang X (2009) J Electroanl Chem 628:73
61. Minakshi M, Singh P, Thurgate S, Prince K (2006) Electrochem Solid State Lett 9(10):A471
62. Wang F, Liu Y, Liu C-Y (2010) Electrochim Acta 55:2662
63. Kohler J, Makihara H, Uegaito H, Inoue H, Toki M (2000) Electrochim Acta 46:59
64. Wang GJ, Zhang HP, Fu LJ, Wang B, Wu YP (2007) Electrochem Commun 9:1873
65. Wang GJ, Qu QT, Wang B, Shi Y, Tian S, Wu YP, Holze R (2009) J Power Sources 189:503
66. Wang H, Zeng Y, Huang K, Liu S, Chen L (2007) Electrochim Acta 52:5102
67. Wang H, Huang K, Zeng Y, Zhao F, Chen L (2007) Electrochem Solid-State Lett 10(9):A199
68. Stojkovic I, Cvjeticanin N, Pašti I, Mitric M, Mentus S (2009) Electrochem Commun 11:512
69. Wang Y, Shang H, Chou T, Cao G (2005) J Phys Chem B 109:11361
70. Ng SH, Chew SY, Wang J, Wexler D, Tournayre Y, Konstantinov K, Liu HK (2007) J Power Sources 174:1032
71. Wang GX, Zhong S, Bradhurst DH, Dou SX, Liu HK (1998) J Power Sources 74:198
72. Reiman KH, Brace KM, Gordon-smith TJ, Nandhakumar I, Attard GS, Owen JR (2006) Electrochem Commun 8:517
73. Wu M-S, Wang M-J, Jow JJ, Yang W-D, Hsieh C-Y, Tsai H-M (2008) J Power Sources 185:1420
74. Wang H, Huang K, Zeng Y, Yang S, Chena L (2007) Electrochim Acta 52:3280
75. Luo JY, Xia YY (2007) Adv Funct Mater 17:3877
76. Liu X-H, Saito T, Doi T, Okada S, Yamaki J-I (2009) J Power Sources 189:706
77. Wang GJ, Yang LC, Qu QT, Wang B, Wu YP, Holze R (2010) J Sold Sate Electrochem 14:865
78. Feldberg SW (1984) J Am Chem Soc 106:4671
79. Meada Y (1990) J Electrochem Soc 137:3047